High Energy Density Physics 9 (2013) 578–582

Contents lists available at SciVerse ScienceDirect

High Energy Density Physics

journal homepage: www.elsevier.com/locate/hedp

Collimated quasi-monoenergetic electron beam generation from intense laser solid interaction

W.M. Wang [a], L.M. Chen [a,*], J.Y. Mao [a,b], K. Huang [a], Y. Ma [a], J.R. Zhao [a], L. Zhang [a], W.C. Yan [a], D.Z. Li [c], J.L. Ma [a], Y.T. Li [a], X. Lu [a], Z.Y. Wei [a], Z.M. Sheng [a,d], J. Zhang [a,d]

[a] Beijing National Laboratory for Condensed Matter Physics, Institute of Physics, CAS, Beijing 100190, China
[b] University of Kaiserslautern and Research Center OPTIMAS, Kaiserslautern 67663, Germany
[c] Institute of High Energy Physics, CAS, Beijing 100049, China
[d] Laboratory for Laser Plasmas (Ministry of Education) and Department of Physics, Shanghai Jiao Tong University, Shanghai 200240, China

ARTICLE INFO

Article history:
Received 17 May 2013
Accepted 17 May 2013
Available online 27 May 2013

Keywords:
Laser–solid interaction
Particle-in-cell simulation
Quasi-monoenergetic
Collimated electron beam
Preplasma

ABSTRACT

A quasi-monoenergetic electron beam with divergence of 3° and energy peak of 1 MeV is observed along the target surface from interaction of a bulk Cu target and an intense relativistic laser pulse of 1 TW and 70 fs at a grazing incident angle. A preplasma formed by high-contrast picosecond prepulse plays a crucial role. Particle-in-cell simulations broadly reproduce the result and show that a preplasma with the proper density and a large angle of incidence is required. The preplasma sets up a static electric field along the surface can accelerate electrons. The static electric field is formed just after the passage of the laser. This approach can be extended to higher intensities to generate higher energy beams.

1. Introduction

The fast ignition concept [1] stimulated an impressive body of work on the generation of fast electron emission from laser–solid interactions [2–14]. Experiments [2–8] and simulations [15–17] have shown that the fast electrons emitted at an angle between laser angle of incidence and the target normal direction are due to mechanisms such as resonance absorption, vacuum heating and $J \times B$ heating. By using a reentrant cone target a 1000-fold increase in neutron yield has been achieved [18,19]. So, experiments of obliquely incident laser–solid interaction were performed to investigate the fast electron generation and propagation problems along the inner cone surface.

Recently, fast electron jets were observed along the target surface [9–12]. These surface fast electron (SFE) beams appears when an intense laser pulse is incident at an angle that is large compared to the target normal. Theoretical work [20,21] indicate that when the femtosecond laser is intense and incident angle is sufficiently large, the electron current layer is trapped on the target surface and a strong quasi-static electromagnetic field is formed, thus the preheated fast electrons are confined in this traveling field and is accelerated by the reflected light further along the target surface. The experimental and theoretical works cited above successfully revealed the electron behavior in the cone. However, SFE beams produced in this way have a large divergence angle and the energy spectra exhibit a Maxwellian distribution.

In a previous experiment [22] we showed that by increasing the angle of incidence and controlling the preplasma parameters we could achieve surface electron guiding with a peaked spectrum, which was much narrower than a Maxwellian distribution. Here, we prove that when a well designed laser pulse incident onto a solid target at an angle of incident ~72°, a highly collimated electron beam with divergence angle as small as 3° and a charge of 0.1 nC is created along the target surface and its energy spectrum is no longer Maxwellian. The extraordinary small divergence and slightly peaked spectrum suggest a different acceleration mechanism, and further, this is a first attempt to accelerate particles in a near critical density plasma. The experimental optimization and a theoretical explanation are provided below.

* Corresponding author.
E-mail address: lmchen@iphy.ac.cn (L.M. Chen).

1574-1818/$ – see front matter © 2013 Elsevier B.V. All rights reserved.
http://dx.doi.org/10.1016/j.hedp.2013.05.011

2. Discussion of the experiment

The experiments were performed by using a Ti:sapphire laser operating at a center wavelength of 800 nm. The energy of the laser irradiating the target surface is approximately 240 mJ per pulse. Fig. 1 shows the experimental layout. A *p*-polarized laser beam with duration $\tau_0 = 67$ fs was focused by an *f*/3.5 off-axis parabolic mirror obliquely incident onto a flat Cu target disk of 50 mm diameter and 6 mm thick. The full width at half maximum (FWHM) of the laser focal spot was measured to be ~ 7 μm, which results in an average laser intensity of 2.2×10^{18} W/cm^2. The temporal contrast at tens of picosecond before the main pulse is 10^{-9}, which means that the laser pulse ASE is small. By adjusting the Pockels cell, an intensity-controllable prepulse was added 7 ns before the main pulse to produce a uniform preplasma. An electron spectrometer with 0.1 T magnetic field was set along the target surface direction at approximately 5° from the target surface and 147 mm away from the focal spot to measure the electron energy spectrum from 5 keV to 2 MeV. A stack of four image plates (IPs) (Fujifilm BAS-SR 2025, calibrated in Ref. [23]) with a 100 μm-thick aluminum filter in front, was placed perpendicular to the target surface at the far edge of the target to collect the electrons traveling near parallel to the surface. By using the CASINO Monte Carlo program [24], we calculated the energy-dependent penetration depth of electrons that are incident onto the Al filter and IPs stack. According to the calculation, the four IPs can stop electrons with energies 0.15 MeV, 0.5 MeV, 0.8 MeV and 1 MeV from front to back, respectively. In addition, we use a single-photon-counting X-ray CCD with a knife-edge to measure the preplasma scale length [25].

By optimization of the parameters of the relativistic intensity laser pulses at grazing incident angle on a Cu target, we could obtain highly collimated and reproducible quasi-monoenergetic electron beams along the target surface. Fig. 2(a) shows the spatial distribution of the emitted target surface electron jet, which is achieved in case of the laser incident angle of 72° and an appropriate ns prepulse. The ns laser contrast that is defined as the ratio of the 7 ns prepulse to the main laser pulse is 10^{-5}. We observe that electrons with energy above 0.15 MeV form a small spot on the second IP and get smaller for deeper level in the stack. At the 4th IP layer, which records electrons of energy $E_k > 0.8$ MeV, the divergent angle of the SFE beam is calculated to be 3°. Fig. 2(b) exhibits the angular distribution in polar coordinate of emitted electrons is obtained from the signals of the second IP of the stack along the target surface, whereone observes that the profile of the target surface electrons is intense and highly collimated. For the same shot, the corresponding energy spectrum was detected from the electrons passing through the hole on the IP stack, as shown in the Fig. 2(c), which shows a non-Maxwellian distribution with a slight peak at 0.6 MeV and a sharp cutoff.

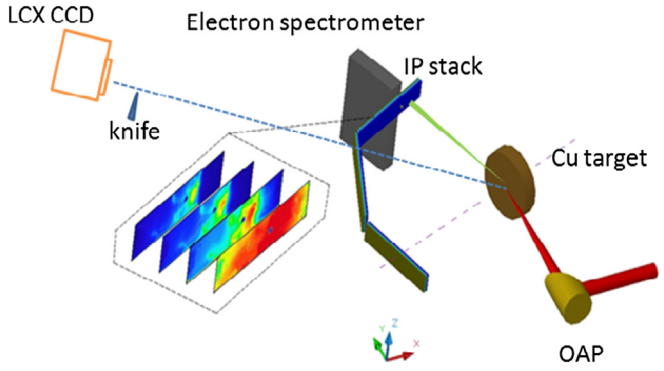

Fig. 1. Experimental setup.

In order to confirm the quasi-monoenenrgetic distribution of the spectrum, we calculated the photo-stimulated luminescence (PSL) values, which are a measure of the intensity of the electron signal, on the IPs in Fig. 2(a) and obtained the electron spectrum shown as a histogram. From Fig. 2(d), the number of the target surface electrons whose energy is above 0.8 MeV is larger than that of electrons whose energies are between 0.5 MeV and 0.8 MeV. This indicates that there is a monoenergetic peak above 0.8 MeV, which is corresponds with our experimental results.

3. Simulations

Emission of electrons along the target surface has been observed in Refs. [9,11] when an intense relativistic laser pulse irradiates a solid target at an oblique angle of incident. This surface emission is responsible for generation of surface static electric fields and magnetic fields. However, the energy spectra of electrons in these previous works are of a Maxwellian type. A new physical picture needs to present to explain the formation of quasi-monoenergetic spectrum observed in our experiments. In the following we comment on a set of particle-in-cell (PIC) simulations that were performed to clarify this question.

The PIC code employed includes two-dimensional (2D) coordinates (x, y) and full momentum space. In the simulations, we simulate an 800-nm-wavelength, p-polarized laser pulse with a FWHM duration of 70 fs and a FWHM spot size of 7 μm. We use a peak intensity of $I = 4 \times 10^{18}$ W/cm^2, i.e., power of 1.14TW and energy of 240 mJ, and an angle of incidence $\theta = 80°$ as standard laser parameters, unless otherwise specified. We take a 4λ thick plasma slab with a density of $10n_c$ and a 10λ thick preplasma in the front of the plasma, where λ is the laser wavelength and $n_c = 2.14 \times 10^{21}$ cm^{-3} is the critical density. The plasma and preplasma are uniform along the x direction and the vacuum-preplasma boundary is located at $y = 65\lambda$. We take the preplasma density n_e of $0.5n_c$ as a standard parameter, unless otherwise specified. The high-density plasma slab prevents the passage of the laser pulse. Actually, the laser pulse with $\theta = 80°$ is reflected at a very small depth in the preplasma of $0.5n_c$ in our simulations, which is in agreement with the critical density $\cos^2\theta n_c(1 + a_0^2/2)^{1/2}$ at the reflected point for an oblique laser, where a_0 is normalized laser field strength.

A quasi-monoenergetic electron beam emitting along the surface is observed in the simulation with the standard parameters, as shown in Fig. 3. The quasi-monoenergetic peak is about 3 MeV, the FWHM divergence angle is around 20° at 0.59 ps, and it has a FWHM size of about 24 μm along the x direction. Here, we only count the electrons moving in the $+x$ direction, with energies >0.5 MeV and near the surface, i.e., $63\lambda < y < 67\lambda$. One can see from Fig. 3(c) and (d) that the beam is mainly located at the surface and travels along the surface, i.e., the $+x$ direction. We increase preplasma density and find that the divergence is reduced and while the quasi-monoenergetic peak disappears gradually. Actually, the quasi-monoenergetic peak appears only when the preplasma density is between $0.2n_c$ and $0.6n_c$, as observed in Fig. 4(a). Also, this peak occurs only with $\theta \geq 72°$, as displayed in Fig. 4(b).

We use Fig. 5 to explain the dependence of the quasi-monoenergetic peak on the preplasma density and the incidence angle. The quasi-monoenergetic beam starts to form at 0.48 ps, see Fig. 3(a), and disappear at 0.64 ps. The second column in Fig. 5 is a typical result during the quasi-monoenergetic beam formation at 0.59 ps. At this time, the reflected laser pulse has just left the target surface, see Fig. 5(a) and (b), and a static electric field $<E_x>$ along the surface is formed in the ion hole bored by the pulse, as shown in Fig. 5(k). The leading edge of $<E_x>$ is at the deceleration phase and the lagging edge of the field, which has a size of about 30λ along the x direction, at the acceleration phase. Such a static field acts like a

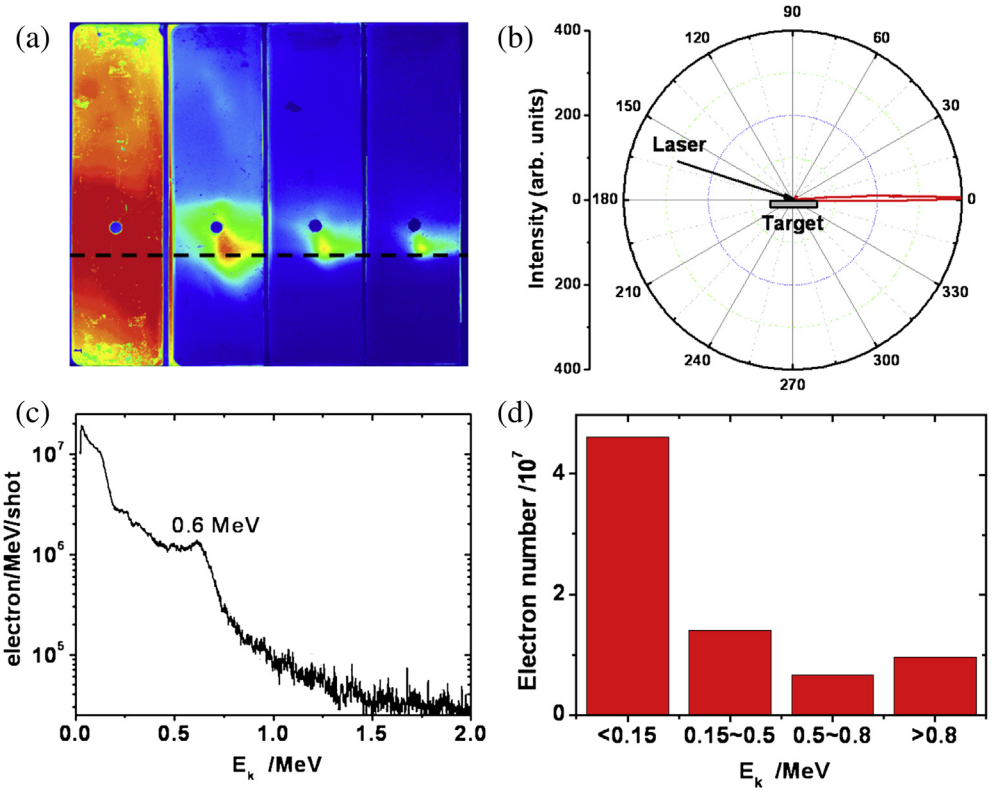

Fig. 2. In the case of low ns laser contrast and large incident angle of 72°, (a) the angular distribution of target surface electrons on IP, (b) the angular distribution in polar coordinate of emitted electrons is obtained from the signals of the second IP of each stack that subtended from the target surface direction, target normal direction and laser reflection direction, (c) the energy spectrum of the target surface electrons, (d) the energy spectrum in histogram of the target surface electrons.

wakefield [26] can accelerate the electrons on the surface [see Fig. 5(f) and notice that the red color denotes the return current along the ion hole] and produce a quasi-monoenergetic beam. At earlier times, this acceleration process does not occur because the laser field dominates the electron production and hence the quasi-monoenergetic peak starts to form just after the laser pulse decreases substantially. Note that such this static field structure can be maintained for less than 0.1 ps, as observed in our simulation, due to the lifetime of the ion hole, which is plotted in Fig. 5(i). More and more background electrons come to the ion hole and form a

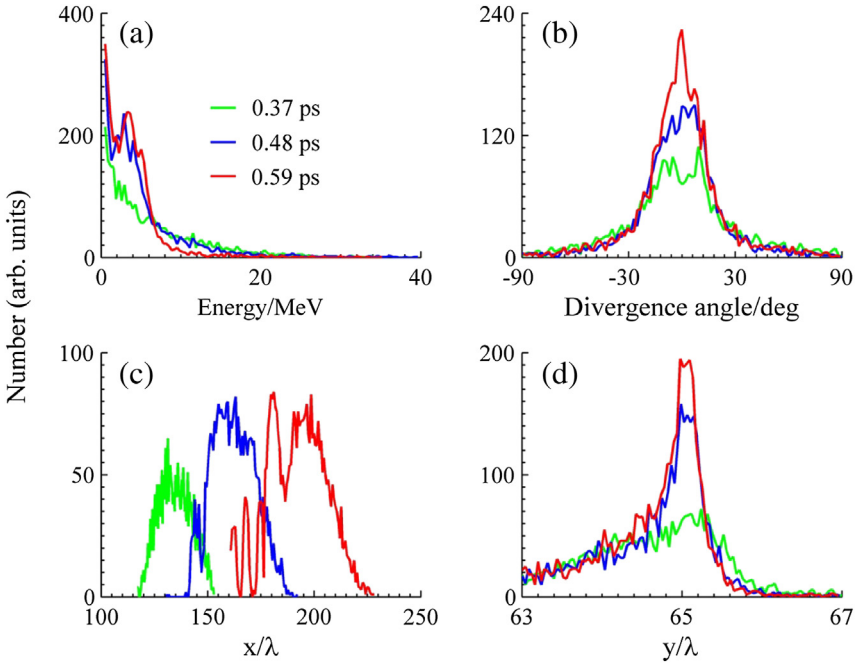

Fig. 3. PIC results. Energy spectra, angle distributions and special distributions of electrons with energy higher than 0.5 MeV and around the target surface at different time.

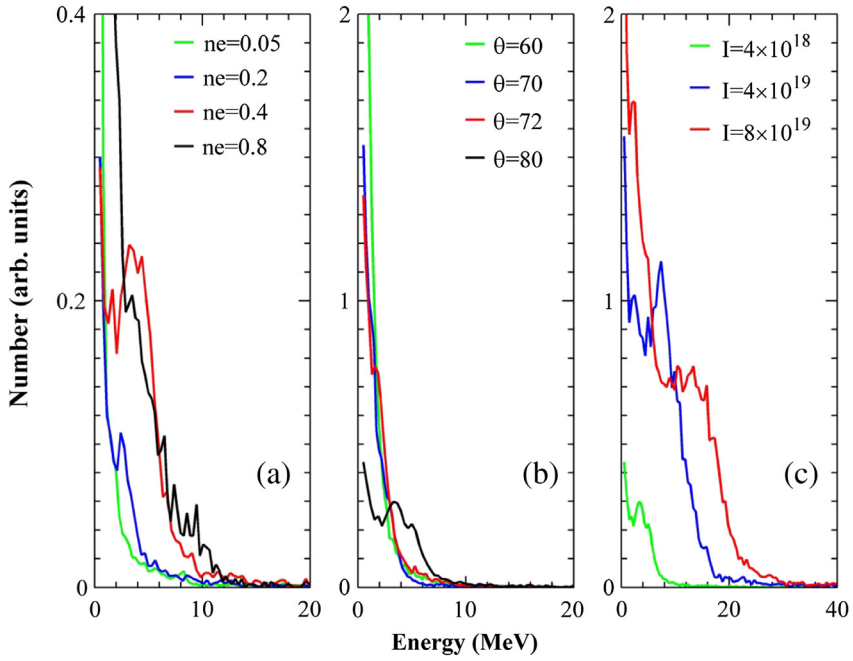

Fig. 4. PIC results. Energy spectra of electrons around the target surface with different preplasma densities [unit of n_c] (a), different incident angles [unit of degree] (b), and different intensities [unit of W/cm^2] (c), where the preplasma density of $0.8n_c$ is taken with intensities of 4×10^{19} and 8×10^{19} W/cm^2 in (c).

complex return current structure, see Fig. 5(g) that corresponds to a complex static field structure shown in Fig. 5(i). Similarly, Fig. 5(h) and (m) illustrate a complex static field structure and return current when the laser field is small because a higher preplasma density of $n_e = 0.8n_c$ is used, so that a clean ion hole is more difficult to form and has a shorter lifetime. As a result, no quasi-monoenergetic beam is observed with relatively high densities. In our simulation, a static magnetic field and a static field along the normal in Fig. 5(j), (b)–(d) are also seen to collimate electrons along the surface. Such collimation fields are strong with relatively high-density preplasma and large angle incidence [9,11] and therefore, collimated and quasi-monoenergetic beams cannot be formed at

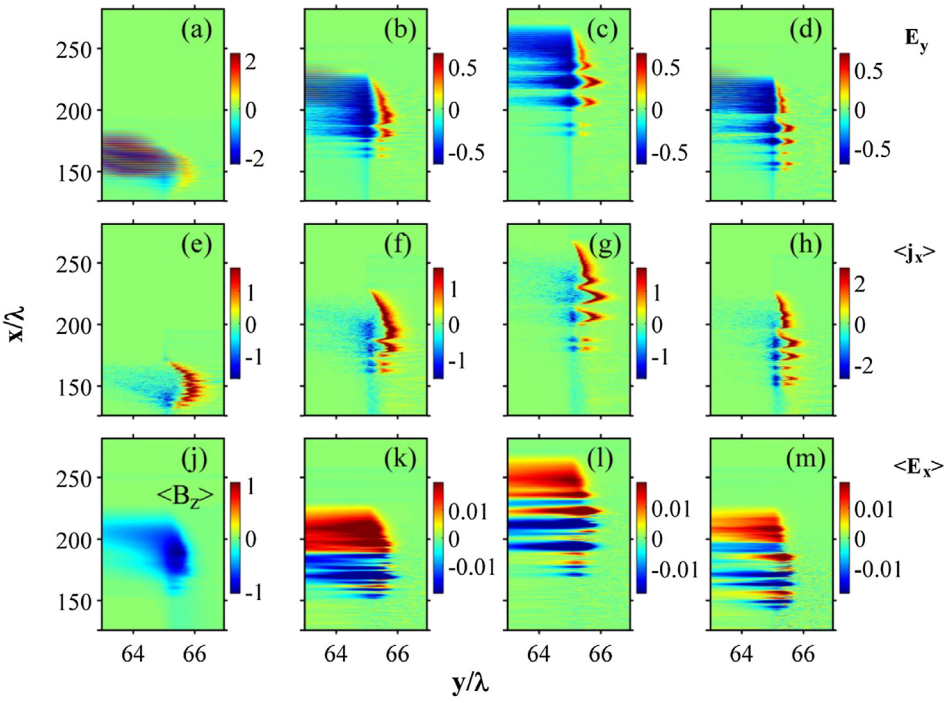

Fig. 5. PIC results. Spatial distributions of fields [unit of $mc\,\omega/e$] and current densities [unit of $10^4 \times ecn_c$], where the first row denotes electric fields along the target normal, the second one temporal average current densities along the surface, and the third one temporal average electric fields along the surface [except (j)]. The first three columns are the results with the preplasma density of $0.5n_c$ obtained at the time of 0.426, 0.586 and 0.693 ps, respectively. The last column at 0.586 ps with the preplasma density of n_c. Plot (j) is the temporal average magnetic field normal to the interaction surface at 0.586 ps.

low densities and at relatively small incident angles. In addition, such quasi-monoenergetic surface beams with higher energies can be generated by higher intensity lasers interacting with higher density preplasmas, as seen in Fig. 4(c).

4. Conclusions

In summary, a MeV quasi-monoenergetic electron beam with 3° divergence angle has been observed along a Cu target surface when a *fs* laser pulse of 1 TW with appropriate ns prepulse and at a 72° angle of incident. The PIC simulation has shown that the quasi-monoenergetic peak is produced by a static electric field along the surface, which forms just after the passage of the laser. A quasi-monoenergetic beam of 10 MeV has been demonstrated by PIC simulation by use of a 10 TW laser. Such electron beams maybe applied in ICF experiments with cone target and in the next generation of accelerator as new type of photocathode.

References

[1] M. Tabak, J.H. Hammer, M.E. Glinsky, et al., Phys. Plasmas 1 (1994) 1626.
[2] S. Bastiani, A. Rousse, J.P. Geindre, et al., Phys. Rev. E 56 (1997) 7179.
[3] M.H. Key, M.D. Cable, T.E. Cowan, et al., Phys. Plasmas 5 (1998) 1966.
[4] Y. Sentoku, H. Ruhl, K. Mima, et al., Phys. Plasmas 6 (1999) 2855.
[5] T.E. Cowan, M. Roth, J. Johnson, et al., Nucl. Instrum. Methods Phys. Res. Sect. A 455 (2000) 130.
[6] M.I.K. Santala, M. Zepf, I. Watts, et al., Phys. Rev. Lett. 84 (2000) 1459.
[7] Y.T. Li, J. Zhang, L.M. Chen, et al., Phys. Rev. E 64 (2001) 046407.
[8] L.M. Chen, J. Zhang, Y.T. Li, et al., Phys. Rev. Lett. 87 (2001) 225001.
[9] Y.T. Li, X.H. Yuan, M.H. Xu, et al., Phys. Rev. Lett. 96 (2006) 165003.
[10] Z. Li, H. Daido, A. Fukumi, et al., Phys. Plasmas 13 (2006) 043104.
[11] H. Habara, K. Adumi, T. Yabuuchi, et al., Phys. Rev. Lett. 97 (2006) 095004.
[12] L.M. Chen, M. Kando, M.H. Xu, et al., Phys. Rev. Lett. 100 (2008) 045004.
[13] A.G. Mordovanakis, J. Easter, N. Naumova, et al., Phys. Rev. Lett. 103 (2009) 235001.
[14] W.T. Wang, J.S. Liu, Y. Cai, et al., Phys. Plasmas 17 (2010) 023108.
[15] Z.M. Sheng, Y. Sentoku, K. Mima, et al., Phys. Rev. Lett. 85 (2000) 5340.
[16] H. Ruhl, Y. Sentoku, K. Mima, et al., Phys. Rev. Lett. 82 (1999) 743.
[17] R. Kodama, K.A. Tanaka, Y. Sentoku, et al., Phys. Rev. Lett. 84 (2000) 674.
[18] R. Kodama, et al., Nature (Lond.) 412 (2001) 798.
[19] R. Kodama, et al., Nature (Lond.) 418 (2002) 933.
[20] T. Nakamura, S. Kato, H. Nagatomo, et al., Phys. Rev. Lett. 93 (2004) 265002.
[21] M. Chen, Z.M. Sheng, J. Zheng, et al., Opt. Express 14 (2006) 3093.
[22] J.Y. Mao, L.M. Chen, X.L. Ge, et al., Phys. Rev. E 85 (2012) 025401. (R).
[23] K.A. Tanaka, T. Yabuuchi, T. Sato, et al., Rev. Sci. Instrum. 76 (2005) 013507.
[24] D. Drouin, A.R. Couture, D. Joly, et al., Scanning 29 (2007) 92.
[25] L.M. Chen, P. Forget, S. Fourmaux, et al., Phys. Plasmas 11 (2004) 4439.
[26] T. Tajim, J.M. Dawson, Phys. Rev. Lett. 43 (1979) 267.